Journal of Materials Chemistry A

Accepted Manuscript

ROYAL SOCIETY OF CHEMISTRY

www.rsc.org/materialsA

Journal of Materials Chemistry A

ARTICLE

Design and Control of Lewis Acid Sites in Sn-substituted Microporous Architectures

Received 00th January 20xx,
Accepted 00th January 20xx

DOI: 10.1039/x0xx00000x

www.rsc.org/

Khaled M. H. Mohammed,[a,b,c†] Arunabhiram Chutia,[a,b] June Callison,[a,b] Peter P. Wells,[a,b] Emma K. Gibson,[a,b] Andrew M. Beale,[a,b] C. Richard A. Catlow[a,b] and Robert Raja[d*]

Monometallic and bimetallic tin-containing framework architectures have been prepared by hydrothermal methods. Structural and spectroscopic techniques were used to probe the nature of the solid-acid sites, at the molecular level, using a combination of XRD, DR UV-Vis, solid state MAS NMR (^{119}Sn, ^{27}Al and ^{31}P) and XAFS. The nature and strength of the solid-acid sites were experimentaly probed by FT-IR spectroscopy using CD_3CN as a probe molecule. To elucidate further the local-structure, the structural characteristics of the Sn sites were probed using DFT calculations, with a view to rationalising the experimental findings. These detailed structural and spectroscopic studies revealed the presence of multiple Sn environments, with the monometallic SnAlPO-5 catalyst displaying a greater number of tetrahedral Sn(IV) active centres. These framework Sn(IV) centres generated stong Lewis acid sites, when compared with their bimetallic Co-Sn analogue, thereby affording attractive possibilities for modulating catalytic reactivity.

Introduction

Tetrahedral (T_d) sites in microporous solids are widely reported as catalytic active centres in selective oxidation and acid-catalysed transformations,[1–4] of which Ti in TS-1,[5] Fe in ZSM-5[6] and Co in AlPO-5[7] are significant examples. Controlling the nature of these active sites allows one to tune the Lewis[8] and Brønsted acidity,[9] and regulate redox[10] centres for oxidation catalysis. The addition of a second heteroatom allows for further optimisation of these properties, as well as influencing the coordination geometry of the initial heteroatom.[2–4]

The incorporation of Sn into zeolitic[11] and non-zeolitic[1,4] architectures has received significant attention for its promising performance in Baeyer-Villiger oxidations.[11] The activity of these systems was correlated with the presence of Sn in T_d sites, with well isolated Lewis acidic centres, which can be used for a wide range of catalytic reactions.[11–13] The synthetic findings were supported by a large number of characterization techniques, including DR UV-Vis, ^{119}Sn MAS NMR and *in situ* IR spectroscopy.[11,14] Although such materials could be expected to show significant catalytic functionality, the incorporation of Sn into AlPO-5 frameworks in T_d sites is, however, very limited and poorly understood.

This work focuses on the isomorphous substitution of P(V) with Sn (IV) within AlPO-5 using a modified hydrothermal preparation method.[4] Cobalt (Co^{2+}/Co^{3+}) ions can be simultaneously introduced into the AlPO-5 architecture[2,3,15] by the substitution of (Al^{3+}) sites. Recently, a combined DFT and EXAFS study demonstrated the potential of effecting catalytic synergy in Co–Ti bimetallic nanoporous frameworks.[16] However, the prospects of introducing a relatively heavier element like Sn, alongside a redox transition-metal such as Co, could pave the way for probing bifunctional catalytic transformations. Nevertheless, the structural and spectroscopic features of such a system needs to be probed in meticulous detail, for the potential exploitation of such bimetallic framework architectures in catalysis and other energy-based applications.

Experimental

Materials

$SnCl_4$. $5H_2O$ (≥98%), was used as Sn source; H_3PO_4 (85 wt% in H_2O), as P source; $Co(CH_3COO)_2$. $4H_2O$ (≥98%), as Co source; $Al(OH)_3$. xH_2O, as Al source and N,N-dicyclohexylmethyl amine (≥97%), as the SDA. All chemical reagents are sigma-Aldrich grade and were used as received.

Catalyst preparation

The syntheses of the isomorphously substituted 3 mol% Sn and 6 mol% CoSn (1:1) into AlPO-5 framework are based on

[a] UK Catalysis Hub, Research Complex at Harwell (RCaH), Rutherford Appleton Laboratory, Harwell Oxon, OX11 0FA (UK).
[b] Department of Chemistry, University College London, 20 Gordon Street, London, WC1H 0AJ, UK.
[c] Chemistry Department, Faculty of Science, Sohag University, Sohag, P.O.B 82524, Egypt.
[d] School of Chemistry, University of Southampton, Southampton, SO17 1BJ (UK).
† Corresponding authors: Robert Raja (R.Raja@soton.ac.uk) and Khaled Mohammed (khaled.mohammed@rc-harwell.ac.uk).
Electronic Supplementary Information (ESI) available: [details of any supplementary information available should be included here]. See DOI: 10.1039/x0xx00000x

modified synthetic procedures described elsewhere.[4] Typically, 2.8 g of $Al(OH)_3$. xH_2O was added to a homogeneous solution of 6.2 g of H_3PO_4 (85 wt% in H_2O) in 6.88 ml of water which resulted in the formation of a viscous white gel. Then, a further 6.88 ml of H_2O was added to the reaction mixture and allowed to stir for 10 min. An aqueous homogeneous solution of $SnCl_4$. $5H_2O$ (0.38 g in 6.88 ml of H_2O and sonicated for 5 min) was added to the above solution (in the case of 6 mol% CoSnAlPO-5, solutions containing 3 mol% of Co and 3 mol% of Sn were prepared individually by the same way and added simultaneously to the reaction mixture). The solution was then kept under constant vigorous stirring for 30 min in order to get a homogeneous gel. Subsequently, 5.61 g of SDA (N,N-dicyclohexylmethyl amine) was added dropwise to the reaction mixture within 10-15 min followed by the addition of the remaining amount of water to maintain the reaction mixture with the following gel composition; 1Al : 1.5P : 0.03Sn : 0.80SDA : $60H_2O$ (in the case of 6 mol% CoSnAlPO-5, the gel composition was; 1Al : 1.5P : 0.03Co : 0.03Sn : 0.80SDA : $60H_2O$). The mixture was then kept under vigorous stirring for further 30 min. Finally, the gel was transferred and sealed into Teflon-lined stainless-steel autoclave, which was then heated to 180 °C under autogenously pressure for 2 h. The solid product was collected by filtration, washed with approx. 1000 ml of deionized water and dried overnight at 100 °C. The dried samples are denoted as 3%Sn-D and 6%CoSn-D. Finally, and to remove the SDA, the samples were calcined in a flow of compressed air for 12 h at 700 °C (5 °C/min). The calcined samples are denoted as 3%Sn-700C and 6%CoSn-700C. We note that calcination at 550 °C, which is commonly used for removing the SDA from AlPO-5 based materials, was given a first trial. However, this temperature was not enough to remove completely the SDA and a grey/oily solid powder was obtained (see Fig. S1 in ESI file). So, based on the TGA analysis (see Fig. S2 and S3 in ESI file) the samples were calcined at 700 °C. A detailed gel composition, synthesis conditions and elemental analysis are summarized in Table 1.

Characterization

The X-ray diffraction patterns were collected between 5-40° of 2θ at a step size of 0.02° on a MiniFlex 300/600, Rigako diffractometer using Cu $K_{\alpha 1}$ radiation, λ=1.54056 Å. ^{119}Sn, ^{31}P and ^{27}Al MAS NMR spectra were measured on Bruker Avance III HD or Varian VNMRS spectrometer (400.177 MHz ^{119}Sn frequency, 161.99 MHz ^{31}P frequency and 104.19 MHz ^{31}Al frequency). $Sn(CH_3)_4$, H_3PO_4 (85 wt%) and $Al(NO_3)_3$ (1M aq. solution) were used as external references for ^{119}Sn, ^{31}P and ^{27}Al spectra, respectively (see ESI file for detailed experimental conditions). DR UV/Vis spectra were collected using a UV-Vis 2600 spectrometer with an integrated sphere in the range of 200-800 nm. The baseline was corrected by using blank $BaSO_4$ discs before the measurement. Measurements were performed on the calcined and reduced samples (see ESI file). FT-IR spectra were collected with an Agilent Cary 680 spectrometer by taking 64 scans in 4000-650 cm^{-1} with a resolution of 4 cm^{-1} using a liquid nitrogen cooled MCT detector. Self-supporting wafers, 15 (±2) mg of sample, were pressed using a 13 mm Die (1.33 cm^2) and sealed in a Harrick transmission cell fitted with CaF_2 windows. Prior to the measurements, the sample was first heated to 150 °C and held for 2 h in a flow of helium gas to remove the adsorbed water. The sample was then cooled down to room temperature (RT) in the same flow before the exposure to CD_3CN. Several injections of CD_3CN (1 μl/injection) were performed at RT until saturation was obtained. The sample was then heated in 25 °C steps; spectra were recorded after 10 minutes at each temperature. All spectra were normalised to 10 mg of sample wafer.

Sn K edge XAFS spectra were recorded at the B18 beamline at the Diamond Light Source, Didcot, UK. Measurements were performed using a QEXAFS set-up with a fast-scanning Si (311) double crystal monochromator. The time resolution of the spectra was 2 min/spectrum (k_{max} = 14, step size 0.5 eV); on average three scans were acquired to improve the signal to noise level of the data for transmission measurements. All samples were prepared as undiluted pellets (hydrated or dehydrated samples), with the amount of sample optimised to yield a suitable edge step and measured in transmission mode using ion chamber detectors. All XAFS spectra were acquired concurrently with the appropriate foil placed between I_t and I_{ref}. The data processing was performed using IFEFFIT package (Athena).[17] For the dehydration process, the pelletized samples were heated under vacuum at 550 °C at 5 °C/min ramp for 2 h, then cooled down to RT, transferred to a glove box for sampling in an air sensitive sample holder with kapton windows prior to the XAFS measurement.

The DFT calculations were performed using the DMol[3] code. A double numerical plus polarization (DNP) basis set was employed, which is equivalent to 6-31G(d,p) Gaussian basis sets. A PW91 gradient corrected exchange-correlation functional was used. The structures were optimized till the energy, forces and displacements were below 1 × 10^{-5} Ha, 2 ×

Table 1 Gel composition and preparation conditions for the hydrothermal preparation of 3%Sn and 6%CoSn AlPO-5 materials.

Catalyst	Gel composition	pH[a]	Conditions	Conc. (mmol g^{-1})[b]	
				Sn	Co
AlPO-5	Al : P : SDA : H_2O 1:1.5:0.80:60	5.5	Synthesis at 180 °C for 2 h. Drying overnight at 100 °C. Calcination for 12 h at 700 °C (5 °C/min) in compressed air.	--	--
3%Sn	Al:P:Sn:SDA:H_2O 1:1.5:0.03:0.80:60	5.6		0.22	--
6%CoSn	Al:P:Sn:Co:SDA:H_2O 1:1.5:0.03:0.03:0.81:60	5.9		0.20	0.24

[a] pH was measured after the final stirring and before transferring the gel into PTFE liner for crystallization.

[b] conc. was measured by elemental analysis using MP-AES technique.

10^{-3} Ha/Å and 5 × 10^{-3} Å, respectively. In addition to this, a default fine atomic orbital cutoff (4.8 Å) was also adopted. The Sn substituted AlPO-5 structure was modelled using an AlPO-5 framework with 144 atoms, to which periodic boundary conditions were applied. To compensate the charge due to the substitution of Sn in a P site of AlPO-5 we protonated an oxygen atom next to the Sn atom. To mimic hydrated experimental samples, calculations with two water molecules in the vicinity of Sn atom were also performed. For comparative purposes calculations were also performed in presence of three and twelve water molecules. Further experiments suggested the presence of SnO_2 inside the framework, which was modelled by placing an SnO_2 molecule near to a Sn atom in the AlPO-5 frameworks. The Sn–O distances as obtained from these calculations were then compared with those from the EXAFS data.

Results and discussion

XRD

Fig. 1 (A and B) shows the XRD patterns derived from the as-synthesised and calcined samples, respectively. In addition, the diffraction pattern for the undoped AlPO-5 is also presented for comparison. All samples reveal the AlPO-5 structure reported in the literature[18] without any phase impurity. The incorporation of the metal dopants into the AlPO-5 framework does not cause any phase changes and the AlPO-5 framework is maintained. The unit cell parameters are summarised in Table S1 (see ESI file). We see a small expansion in the "a" direction compared to the undoped phase of AlPO-5, indicating that heteroatom incorporation was achieved. The decrease in peak intensity at 19-25° 2-theta, can be attributed to the formation of SnO_x clusters and to the presence of Al in higher coordination environments. Surface areas (S_{BET}, $m^2.g^{-1}$) were obtained to compare the bimetallic and monometallic catalysts (see Table S2 in the ESI file). These results are similar to those obtained for AlPO-5 based materials and confirm their microporous nature. Our XANES results (see later) reveal the presence of SnO_x nanoclusters (possibly within the micropores), in addition to tetrahedral Sn sites, which could well explain the reasons for observed decrease in surface area.

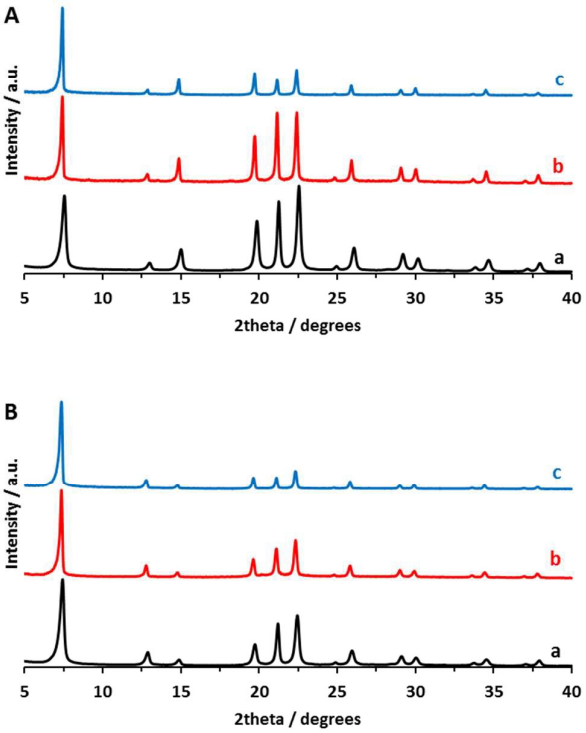

Fig. 1 XRD patterns of A) as-synthesised and B) calcined for a) undoped AlPO-5, b) 3%Sn and c) 6%CoSn substituted materials.

DR UV/Vis

The speciation of the metals has been investigated using diffuse reflectance (DR) UV/Vis (Fig. 2A and B). We focus on two regions of spectrum. The Charge Transfer (CT) region from 200-500 nm and the d-d transitions from 500-800 nm. The 3%Sn-700C sample displays an absorption band with a maximum at ~ 223 nm (Fig. 2A, curve a) which can be ascribed to Sn(IV) species in T_d sites.[1] However, the broad feature of this band down to 300 nm suggests the presence of another Sn(IV) environment in this sample, probably SnO_x nanoclusters.[19] On reduction, this band can be resolved into two components with a maximum at 217 and 244 nm (Fig. 2B, curve a) which confirms the coexistence of multiple Sn(IV) environments. The two absorption bands observed for the 6%CoSn-700C sample with a maximum at ~ 334 and 417 nm

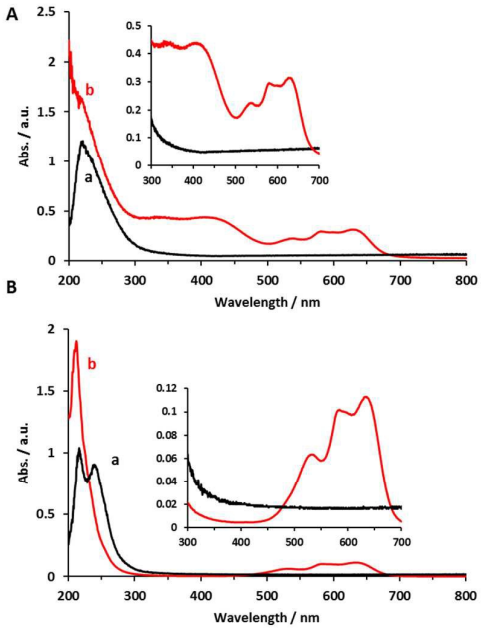

Fig. 2 DR UV-Vis spectra of A) calcined and B) reduced (in a H_2 flow for 2 h at 400 °C, see ESI file) samples of 3%Sn-700C (curve a, black lines) and 6%CoSn-700C (curve b, red lines) samples. Inset graph shows the range of 300-700 nm of wavelength.

(Fig. 2A, curve b) are due to the LMCT transitions of T_d Co(III) sites,[2] while the triplet bands located at ~ 535, 580 and 632 nm (Fig. 2A, curve b) can be assigned to the d-d transitions of Co(II) ions in a T_d coordination. The intensity of the latter bands increased after reduction (Fig. 2B, curve b) suggesting the initial coexistence of Co(II) and Co(III) sites.[2,20] Thus, the DR UV/Vis analysis identifies the predominance of multiple Sn(IV) environments (as T_d sites and SnO_x nanoclusters) in these samples. In addition, it confirms the successful incorporation of both Sn and Co ions into the AlPO-5 framework.

^{119}Sn MAS NMR

^{119}Sn MAS-NMR has been used extensively for probing the nature of Sn species in zeolites,[21–23] and these interpretations can be rationally extended for probing analogous species in AlPO-5. In Fig. 3A, three Sn environments are present in the 3%Sn-700C sample (Fig. 3A, curve a) with clear chemical shifts at -608, -670 and -728 ppm. The first one (at -608 ppm) is assigned to SnO_x clusters and is in agreement with previous reports for SnO_2 species,[21] with the magnitude of this peak being dependent on the degree of SnO_x oligomerization.

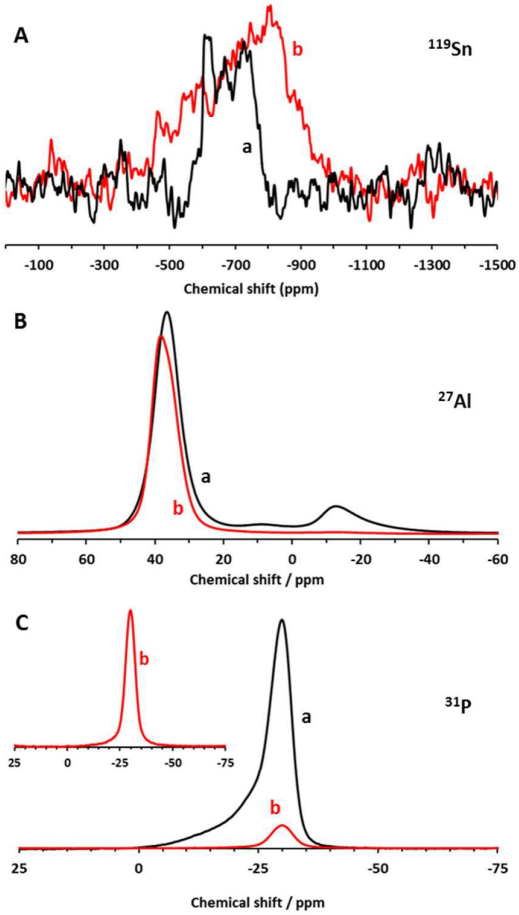

Fig. 3 A) ^{119}Sn, B) ^{27}Al and C) ^{31}P MAS NMR spectra for a) 3%Sn-700C and b) 6%CoSn-700C samples.

However, the other two chemical shifts (at -670 and -728 ppm) are ascribed to hydrated, Sn(IV) species in T_d sites (closed and/or open sites).[11,22,23] There are, however, somewhat broader features in 6%CoSn-700C sample (Fig. 3A, curve b) suggesting also the presence of multiple Sn environments in this sample. In addition, a clear peak emerges at a lower chemical shift with a maximum around -810 ppm, which could be a result of the paramagnetic effect of Co species. As with the DR UV-Vis analysis, the ^{119}Sn MAS NMR spectra show an evidence for multiple Sn species, with the strongest evidence for framework Sn sites present for the 3%Sn-700C sample.

^{27}Al MAS NMR

Fig. 3B (curves a and b) displays the ^{27}Al MAS NMR spectra of 3%Sn-700C and 6%CoSn-700C catalysts, respectively. Both samples are dominated by a peak at ca. 36 ppm, which is typical for ^{27}Al chemical shift, relating to tetrahedrally coordinated Al in AlPO-5 based materials.[24] However, the position of this peak is slightly shifted to a higher chemical shift for 6%CoSn-700C sample, which could be as a result of the successful substitution of Al(III) sites by Co species in this sample. Additionally, in the 3%Sn-700C sample, small peaks were observed at 14 and -13 ppm. Two different interpretations have been reported for these bands. Akolekar *et al*.[24] attributed these bands (14 and -13 ppm) to the presence of non-reacted (extra-framework) Al species in 5- and 6-coordination, respectively. In contrast, Zhao *et al*.[25] reported these signals (14 and -13 ppm) to reacted (framework) T_d Al sites surrounded with one- or two-water molecules, respectively. Interestingly, no evidence for these extra bands was found for 6%CoSn-700C sample and it is plausible that some of these Al(III) sites undergo type 1 substitution (during synthesis) to generate tetrahedral cobalt species in the bimetallic catalyst.

^{31}P MAS NMR

^{31}P MAS NMR analysis has been widely used to probe the isomorphous incorporation of heteroatom atoms in AlPO-5 based frameworks.[26,27] Fig. 3C (curves a and b) shows the ^{31}P MAS NMR spectra for 3%Sn-700C and 6%CoSn-700C samples, respectively. The spectra are dominated by an intense resonance at -30 ppm, denoted as P(4Al), which is characteristic of tetrahedral phosphorus linked to four –OAl groups in AlPOs materials.[28] However, a 3%Sn-700C sample exhibited a low-intensity wide band as a down-field shoulder of the P(4Al) signal, which could be related to the presence of an extra phase. The extension of this low-intensity wide band down to -10 ppm suggesting that non-reacted P species are also present in this sample. There is, however, no evidence for the presence of any non-reacted P species and/or extra Sn phases in 6%CoSn-700C sample.

Sn K edge XAFS analysis

XANES spectra

Identification of Sn within the framework sites was provided by X-ray Absorption Fine Structure, XAFS, (Fig. 4) analysis. The

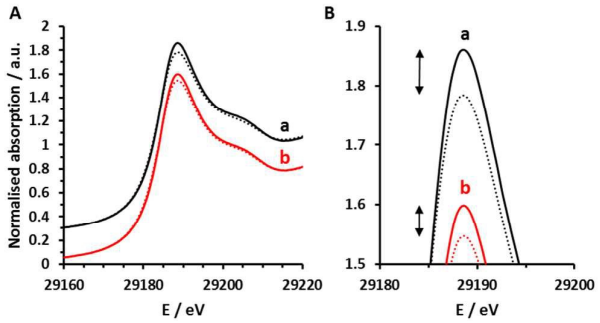

Fig. 4 A) Sn K-edge XANES spectra of hydrated (solid lines) and dehydrated (dotted lines) for a) 3%Sn-700C (black) and b) 6%CoSn-700C (red) samples and B) zooming in of graph A) to show the differences in the main edge intensity between hydrated and dehydrated samples.

X-ray Absorption Near Edge Structure (XANES) is sensitive to both oxidation state and coordination geometry. The XANES spectra of all catalysts were measured under hydrated and dehydrated conditions to assess the amount of Sn within the framework. The spectra for all catalysts have an edge position (29184 eV), which is consistent with that reported for SnO_2, which confirms that the Sn sites are present as Sn(IV) after the calcination process, with no evidence for the presence of any Sn(II) species. Fig. 4A shows the normalised Sn K-edge XANES spectra for the hydrated and dehydrated catalysts. A reduction in XANES intensity after dehydration is expected as the environment moves from O_h to T_d and the oxygen coordination is reduced. Recently, a similar approach was employed to identify the incorporation of Sn within zeolite beta.[29] Based on the difference in main edge intensity of XANES spectra before and after dehydration, it was found that the order of dehydration and by extension the population of framework Sn sites is in the following order: 3%Sn-700C > 6%CoSn-700C (Fig. 4B). However, it should be noted that the difference is much less than would be expected if all Sn sites were incorporated within the framework, which suggests the presence of multiple Sn sites.

EXAFS

To understand better the local environment of the Sn heteroatom, EXAFS analysis of the 3%Sn-700C sample, in hydrated and dehydrated forms was performed. Fig.5 represents the Sn K-edge derived k^3-weighed EXAFS data for hydrated and dehydrated 3%Sn-700C sample in A) k space and B) R space, respectively. The experimental data could be fitted with oxygen at two different distances (1.97-1.98 and 2.06-2.09 Å) and with one tin distance at 3.24-3.25 Å. In addition, a second tin atom could be fitted at a distance of 3.42 Å in the hydrated form of the sample. The fitted parameters are presented in Table 2. Although the XANES analysis confirms the presence of multiple Sn species with fractions of framework Sn sites, the parameters generated from the EXAFS fittings are consistent with the DFT calculations reported below on SnAlPO5 material with/without water molecules.

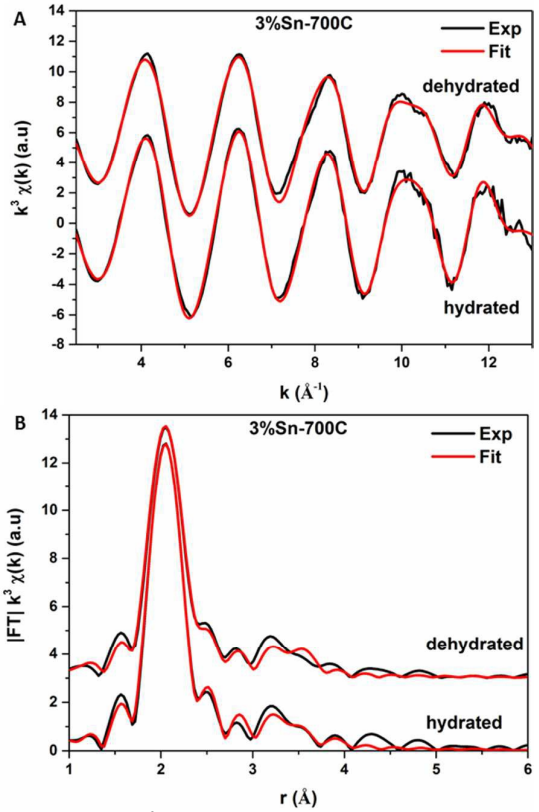

Fig. 5 Sn K-edge derived k^3-weighed EXAFS data for hydrated and dehydrated 3%Sn-700C sample in A) k space and B) R space.

Geometry by DFT

Density functional theory (DFT) calculations have been widely used in combination with EXAFS to reveal the structure of active sites of similar systems.[16] An AFI model was used for all the DFT calculations as shown in Fig. 6. First, we measured various Sn–O bond lengths in Sn substituted AlPO-5 structures.

Table 2 EXAFS fitting parameters for hydrated and dehydrated 3% Sn AlPO5 sample at Sn K edge.

3%Sn-700C	Scattering path	N	σ^2 (Å^2)	ΔE_0 (eV)	r (Å)	R-factor
Hydrated	Sn-O1	2 (1)	0.002 (2)	5.9 (6)	1.97 (2)	0.003
	Sn-O2	4 (1)	0.002 (1)		2.06 (1)	
	Sn-Sn1	1.1 (3)	0.005 (2)		3.25 (2)	
	Sn-Sn2	0.6 (5)	0.007 (7)		3.42 (6)	
Dehydrated	Sn-O1	2.7 (7)	0.002 (1)	6.4 (8)	1.98 (1)	0.005
	Sn-O2	2.8 (7)	0.002 (1)		2.09 (1)	
	Sn-Sn	0.9 (2)	0.005 (2)		3.24 (2)	

Fitting parameters: S_0^2 = 0.93 as deduced by SnO_2 standard; Fit range 2.5<k<13, 1<R<3.5. Values in parenthesis are the experimental error value.

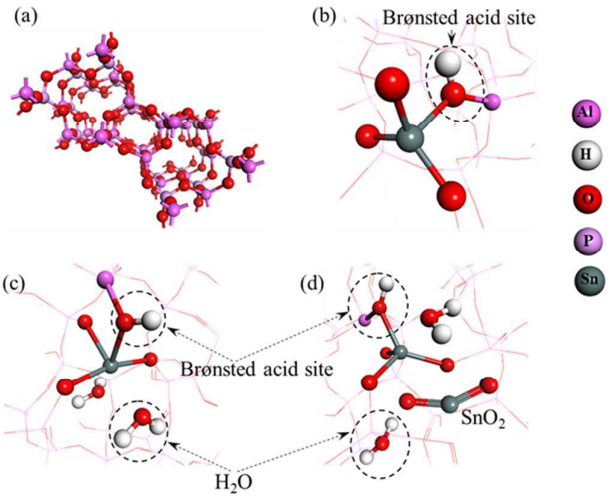

Fig. 6 Configurations modelled using DFT calculations: (a) AFI framework ; (b)) Brønsted acid site without additional water molecules; (c) Brønsted acid site with two water molecules; (d) Brønsted acid site with two water molecules and SnO_2 molecule

The calculations also showed Sn-O bond distances of 1.951 Å (Sn – O) and 2.117 Å (Sn–O_H), where Sn–O_H is for the Sn–O bond length for Sn and the O atom next to the Brønsted acid site, for the unhydrated system and 1.994 Å (Sn – O) and 2.080 Å (Sn–O_H) for the hydrated systems. On the inclusion of an SnO_2 molecule to evaluate Sn–Sn distance in the hydrated system we found that this difference in bond lengths between Sn–O and Sn–O_H became negligible. The Sn–Sn distance between Sn in the framework and Sn of SnO_2 was found to be 3.472 Å, which is also close to the Sn–Sn experimental value of 3.420 Å. We further investigated the Sn–Sn distance in SnAlPO-5 without water molecules (2.948 Å), in presence of two (3.472 Å), three (3.627 Å) and twelve water molecules (3.691 Å) to check how the intermolecular Sn–Sn distance is influenced in their presence. These results showed that the Sn–Sn distance monotonically increases with the number of water molecules but is close to the experimental findings in presence of two water molecules i.e., in an Oh environment. On closely monitoring the Sn–O distances it was evident that with the inclusion of water and SnO_2 molecule there was contraction and expansion in the zeolite framework near the Sn atom. In addition to the above Sn–O distances for the Sn and O atoms next to each other, we also calculated the Sn–O distances between the framework Sn and O of the water molecules. These were found to be in the range of 2.285 – 3.822 Å. The large Sn–O_{H2O} distance of 3.822 Å is due to inter molecular interaction between SnO_2 and the water molecule, which tends to move away from framework Sn to form H-bond with other nearby O atoms of the zeolite framework.

Table 3 Position, area and concentration of strong Lewis (SL), weak Lewis (WL) and Brønsted (B) acid sites.

Catalyst	Wavenumber (cm^{-1})	Acidic site
3%Sn-700C	2323	Strong Lewis acid site
	2308	Weak Lewis acid site
	2285	Brønsted acid site
6%CoSn-700C	2308	Weak Lewis acid site of Co
	2285	Brønsted acid site

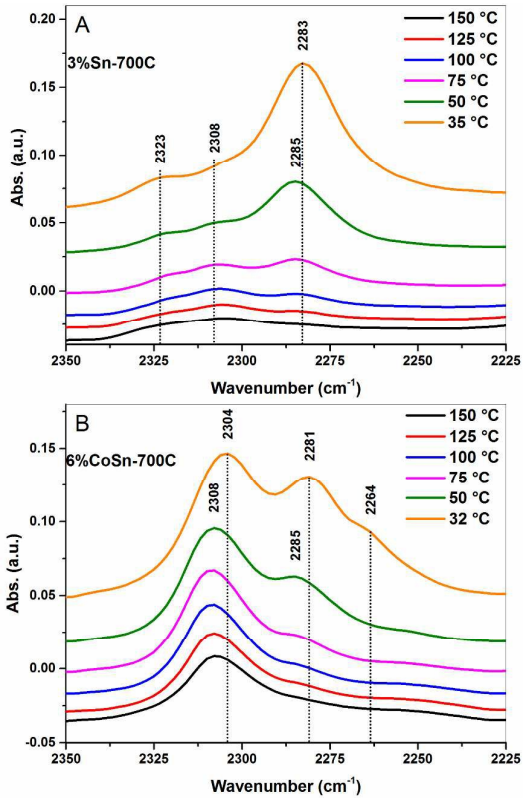

Fig. 7 FT-IR spectra of adsorbed CD_3CN species over A) 3%Sn-700C and B) 6%CoSn-700C catalysts taken at RT, 50, 75, 100, 125 and 150 °C. Spectra have been offset vertically for clarity.

IR experimental results

The nature of acidic Sn sites (Lewis & Brønsted) in 3%Sn-700C and 6%CoSn-700C samples were probed by monitoring the changes in the ν(C≡N) bands of adsorbed d_3-acetonitrile (CD_3CN) in the range of 2240-2360 cm^{-1}.[30] CD_3CN has been chosen as a probe molecule due to its ability to cover all acidic sites in porous materials.[31] The IR spectra for the 3%Sn-700C and the 6%CoSn-700C samples exposed to CD_3CN (Fig. 7 A and B) both show an intense band at 2283-2285 cm^{-1} which can be assigned to the interaction of the C≡N group with Brønsted acid sites. The most striking difference observed for the adsorption of CD_3CN on the 6%CoSn-700C sample is the intense band observed at 2308 cm^{-1}. This band has previously been assigned to a weak Lewis acid site of Co substituted AlPO's.[31] All assignments are summarised in Table 3.The desorption characteristics of the two samples are similar. The CD_3CN on the Brønsted acid sites desorbs on heating to 150°C whilst the CD_3CN adsorbed on the Lewis acid sites is still present.

The additional weak bands observed on the 3%Sn-700C sample at 2323 and 2308 cm^{-1} could be due to strong and weak Lewis acid sites of Sn.[30,31] These bands have previously been assigned to 'hydrolysed' and 'non hydrolysed framework' Sn sites which have been observed at 2316 and 2308 cm^{-1} respectively.[32] The presence of these strong and weak Lewis Sn sites on the Co sample cannot be discounted as these weak bands could easily be hidden by the intense band at 2308 cm^{-1}.

Summary and conclusions

In summary, this study shows the simultaneous incorporation of Sn and Co ions into AlPO-5 framework. In the case of the monometallic system, a greater proportion of Sn(IV) species were incorporated into T_d sites, as evidenced by the XANES and ^{119}Sn MAS-NMR analyses. FTIR spectroscopy further revealed that these tetrahedral Sn centres were the loci for the generation of strong Lewis acid sites (Table 3). The simultaneous isomorphous substitution of Co ions, alongside Sn(IV) centres, modified the acidity of the bimetallic catalyst, resulting in particular in an absence of strong Lewis acid centres. The ability to modulate and control the generation of Lewis and Brønsted acid sites in heterogeneous systems offers potential scope for the rational design of solid catalysts that can be tailored towards a particular catalytic transformation. Our preliminary findings indicate that these catalysts have promising potential in the C-H activation of toluene (to benzaldehyde) and in the oxidation of benzylic alcohols. We believe that the strong Lewis acid sites are implicated in the catalytic oxidation, as observed previously with Sn-Beta zeolites.[11]

Acknowledgements

UK Catalysis Hub is kindly thanked for resources and support provided via our membership of the UK Catalysis Hub Consortium and funded by EPSRC (grants EP/K014706/1, EP/K014668/1, EP/K014854/1 and EP/K014714/1). Also, we would like to thank the EPSRC UK National Solid-state NMR service at Durham for acquiring the Solid-state NMR spectra. The Diamond Light Source and RCaH are thanked for the provision of beamtime (SP10306-1) and the support of their staff. We would like to thank Dr. Gavin Stenning for help on the MiniFlex instrument in the Materials Characterisation Laboratory at the ISIS Neutron and Muon Source. Also, we would like to thank Dr. J. Saßmannshausen for setting up DMol3 for the calculations on the departmental IB-server at UCL.

Notes and references

1 M. Sánchez-Sánchez, R. van Grieken, D. P. Serrano and J. a. Melero, *J. Mater. Chem.*, 2009, **19**, 6833–6841.

2 J. Paterson, M. Potter, E. Gianotti and R. Raja, *Chem. Commun. (Camb).*, 2011, **47**, 517–519.

3 R. M. Leithall, V. N. Shetti, S. Maurelli, M. Chiesa, E. Gianotti and R. Raja, *J. Am. Chem. Soc.*, 2013, **135**, 2915–2918.

4 M. E. Potter, a. J. Paterson and R. Raja, *ACS Catal.*, 2012, **2**, 2446–2451.

5 B. Notari, *Adv. Catal.*, 1996, **41**, 253–334.

6 W. M. Heijboer, P. Glatzel, K. R. Sawant, R. F. Lobo, U. Bergmann, R. A. Barrea, D. C. Koningsberger, B. M. Weckhuysen and F. M. F. de Groot, *J. Phys. Chem. B*, 2004, **108**, 10002–10011.

7 J. Chen, G. Sankar, J. Thomas, R. Xu, G. Greaves and D. Waller, *Chem. Mater.*, 1992, **4**, 1373–1380.

8 G. Sastre and A. Corma, *Chem. Phys. Lett.*, 1999, 302, 447–453.

9 I. Lezcano-Gonzalez, U. Deka, B. Arstad, A. Van Yperen-De Deyne, K. Hemelsoet, M. Waroquier, V. Van Speybroeck, B. M. Weckhuysen and a M. Beale, *Phys. Chem. Chem. Phys.*, 2014, **16**, 1639–50.

10 T. Beutel, J. Sárkány, G.-D. Lei, J. Y. Yan, W. M. H. Sachtler and J. Sa, *J. Phys. Chem.*, 1996, **100**, 845–851.

11 A. Corma, L. T. Nemeth, M. Renz and S. Valencia, *Nature*, 2001, **412**, 423–425.

12 T. M. Abdel-Fattah and T. J. Pinnavaia, *Chem. Commun.*, 1996, 665.

13 N. Kishor Mal, V. Ramaswamy, S. Ganapathy and a. V. Ramaswamy, *Appl. Catal. A, Gen.*, 1995, **125**, 233–245.

14 M. Renz, T. Blasco, A. Corma, V. Fornés, R. Jensen and L. Nemeth, *Chem. - A Eur. J.*, 2002, **8**, 4708–4717.

15 V. Naydenov, L. Tosheva and J. Sterte, *Microporous Mesoporous Mater.*, 2003, **66**, 321–329.

16 M. E. Potter, a. J. Paterson, B. Mishra, S. D. Kelly, S. R. Bare, F. Cora, A. B. Levy and R. Raja, *J. Am. Chem. Soc.*, 2015, **137**, 8534–8540.

17 B. Ravel and M. Newville, *J. Synchrotron Radiat.*, 2005, **12**, 537–541.

18 M. E. Potter, D. Sun, E. Gianotti, M. Manzoli and R. Raja, *Phys. Chem. Chem. Phys.*, 2013, **15**, 13288–13295.

19 G. Pang, S. G. Chen, Y. Koltypin, A. Zaban, S. Feng and A. Gedanken, *Nano Lett.*, 2001, **1**, 723–726.

20 A. M. Beale, G. Sankar, C. R. A. Catlow, P. A. Anderson and T. L. Green, *Phys. Chem. Chem. Phys.*, 2005, **7**, 1856–1860.

21 J. Catalano, A. Murphy, Y. Yao, F. Alkan, N. Zumbulyadis and S. A. Centeno, *J. Phys. Chem. A*, 2014, **118**, 7952–7958.

22 P. Wolf, M. Valla, A. J. Rossini, A. Comas-Vives, F. Núñez-Zarur, B. Malaman, A. Lesage, L. Emsley, C. Copéret and I. Hermans, *Angew. Chemie - Int. Ed.*, 2014, **75**, 10179–10183.

23 W. R. Gunther, V. K. Michaelis, M. a. Caporini, R. G. Griffin and Y. Román-Leshkov, *J. Am. Chem. Soc.*, 2014, **136**, 6219–6222.

24 D. B. Akolekar and R. F. Howe, *J. Chem. Soc. Faraday Trans.*, 1997, **93**, 3263–3268.

25 R. Zhao, Y. Wang, Y. Guo, Y. Guo, X. Liu, Z. Zhang, Y. Wang, W. Zhan and G. Lu, *Green Chem.*, 2006, **8**, 459.

26 P. J. Barrie and J. Klinowski, *J. Phys. Chem.*, 1989, **93**, 5972–5974.

27 D. E. Akporiaye, A. Andersen, I. M. Dahl, H. B. Mostad and R. Wendelbo, *J. Phys. Chem.*, 1995, **99**, 14142–14148.

28 W. Shea, R. B. Borade and A. Clearfield, *J. Chem. Soc. Faraday Trans.*, 1993, **89**, 3143–3149.

29 C. Hammond, D. Padovan, A. Al-Nayili, P. P. Wells, E. K. Gibson and N. Dimitratos, *ChemCatChem*, 2015, n/a–n/a.

30 A. G. Pelmenschikov, R. A. van Santen, J. Janchen and E. Meijer, *J. Phys. Chem.*, 1993, **97**, 11071–11074.
31 B. Wichterlová, Z. Tvarůžková, Z. Sobalík and P. Sarv, *Microporous Mesoporous Mater.*, 1998, **24**, 223–233.
32 M. Boronat, P. Concepción, A. Corma, M. Renz and S. Valencia, *J. Catal.*, 2005, **234**, 111–118.

Modulation of tetrahedral Sn(IV) active sites in framework architectures influences the generation of Lewis and Brønsted acid sites in heterogeneous catalysts